612. Nonlinear analysis of the ripping head power time series

Grzegorz Litak[a,1], Arkadiusz Syta[b], Jakub Gajewski[c], Józef Jonak[c]
[a]Department of Applied Mechanics, Technical University of Lublin,
Nadbystrzycka 36, PL-20-618 Lublin, Poland
[b]Department of Applied Mathematics, Technical University of Lublin,
Nadbystrzycka 36, PL-20-618 Lublin, Poland
[c]Department of Machine Construction, Technical University of Lublin,
Nadbystrzycka 36, PL-20-618 Lublin, Poland
[1] corresponding author, Fax: +48-815250808;
E-mail: *g.litak@pollub.pl*

Abstract. We investigate the power of a ripping head in the process of concrete cutting. Using nonlinear embedding methods we study the corresponding time series obtained during the cutting process. The calculated maximal Lyapunov exponent indicates the exponential divergence typical for chaotic or stochastic systems. The recurrence plots technique has been used to get nonlinear process statistics for identification and description of nonlinear dynamics, lying behind the cutting process.

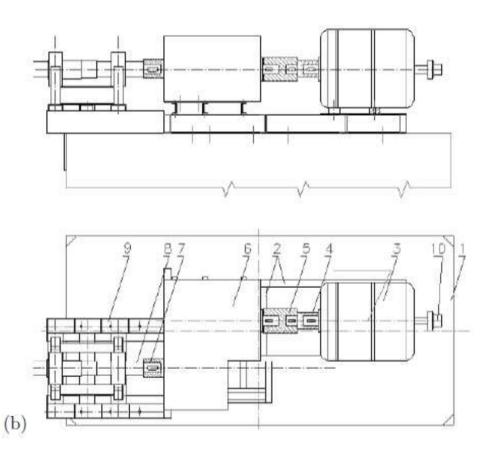**Key words:** ripping head, nonlinear dynamics, vibrations, embedding theory.

1. Introduction

A cutting process, studied experimentally and described theoretically by Merchant [1] in the middle of 20th century, is a highly nonlinear process involving such phenomena as friction, impacts and chips breaking. In case of metal cutting, the most important criterion of its reliability is the high quality of the final product. In practice one has to achieve a compromise between the precision of cutting and cutting costs. Consequently such a process is not designed in a perfect way but it is disturbed by various instabilities including dynamical chatter vibrations. Recently those vibrations have been investigated [2–8] in the context of chaotic motion appearance. Such non-periodic vibrations are very similar to stochastic ones but they have the origin in the nonlinear dynamics of cutting.

Cutting applied to rocks is even more challenging as the machined materials are not uniform and brittle. The main purpose in rock cutting is to achieve maximal efficiency [9, 10] using a relatively small amount of energy. Those priorities lead to the evolution of tools and, in particular, to the technology of multi-tool ripping heads use [11]. In this paper we will present the time series of the ripping head power applied to a standard rock. The application of Recurrence Plots (RP) enabled us to examine the nonlinear properties of the cutting process.

The paper is divided into 5 sections. After the present introduction (Sec. 1) we describe the experimental stand and present a typical example of time series with a short discussion of its properties (Sec. 2). In Sec. 3 we perform the embedding dimension analysis to the studied time series. In Sec. 4 we analyze recurrence plots and make the recurrence plots quantification analysis. Finally in Sec. 5 we end up with conclusions.

39

Fig. 1. Multi-tool ripping head on the test bed (a) and its scheme (b) with the following specification:
1 - Machine foundation; 2 - Frame $\varnothing$ 1600; 3 - Electric motor P=140 kW; 4 - Connector I;
5 - Torque meter; 6 - Reduction gear; 7 - Connector II; 8 - Shaft; 9 - Frame II; 10 - Speed indicator

2. Experimental stand and results

Here we present the results of experiments performed in the test-rig (Fig. 1a). Such experiments are usually conducted to identify the point status of cutting tools in ripping heads of headwall combined cutter-loaders. Rapidly changing mining conditions require an adaptive control procedure to be applied in this process. The conditions of cutting tools, and especially their edges, installed on a multi-tool head are essential in the context of optimization procedure [12].
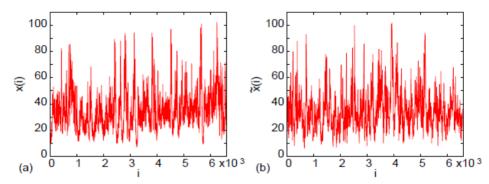

Fig. 2. The measured time series of the power of a ripping head x (a) and the time series of surrogated data $\tilde{x}$ (b) versus time-like measurement index i. The power $x(i)$ (and also $\tilde{x}$ (i)) was expressed in [kW], sampling interval was fixed at $\Delta t = 0.005s$ while the total number of points for the analysis was $N = 6600$. Note that the corresponding standard deviations do not differ so much as $\sigma_x = 14.665$ kW while $\sigma_{\tilde{x}} = 14.688$ kW

The ripping head load measured as the supplied power is rapidly changing in a complex way. Thus the corresponding cutting process is difficult to describe mathematically. A lot of factors can influence the ripping process. The basic group of parameters includes: technology and conditions of excavating, ripping head technical parameters, characteristics of the rock, constructional features of the tool. The scheme and specification of our test stand are presented in Fig. 1b [13].

A system with a full control and automation of the excavating process has not been developed so far. However, the control process, limited to adjusting the ripping speed to current excavating conditions, can be applied. In this process the ripping speed could be estimated through particular parameters of the head drive motor signal. Up to now, the operation of the ripping head depends only on the operator's subjective assessments. It is important at a significant variance in the optimum combined cutter-loader operation. Monitoring the condition of a cutting tool point and the type of a presently installed cutting tool is crucial for the proper multi-tool head operation. The system that will potentially allow to assess the status of the cutting edges and to identify the cutting tool type, e.g. on account of the face of cut and the tool flank, cannot be susceptible to changing qualities of the ripped material [14–16].
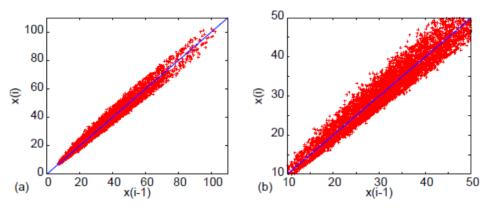
Using the above presented equipment we collected the data of the ripping head power during cutting of a standard concrete (Fig. 1). They are presented as time series in Fig. 2a. In the first sight one can observe that this time history does not exhibit any periodic oscillations. Examining the properties of this representative time series is the main purpose of the current analysis.

41

To check nonlinearity of the time series we have applied a surrogate test [17], which is based on the Fourier transform

$$a_j = \frac{2}{N} \sum_{i=1}^{N} x(i) \cos(i\Delta t \omega_j), \qquad b_j = \frac{2}{N} \sum_{i=1}^{N} x(i) \sin(i\Delta t \omega_j),$$

(1)

where the corresponding amplitude A_j and the frequency ω_j are defined respectively. Δt is the sampling interval.

$$A_j = \sqrt{a_j^2 + b_j^2}, \qquad \omega_j = \frac{2\pi j}{N\Delta t}.$$

(2)

Fig. 3. Return maps in different scales: (a) data in the whole region and (b) data limited the chosen interval (from 10 to 50 kW). Figure (b) shows the noticeable broken reflection symmetry with respect to the diagonal line

After adding random passes ϕ_j to terms with ω_j one can calculate the inverse transform

$$\tilde{x}(i) = \frac{a_0}{2} + \sum_{j}^{N/2} A_j \sin(\omega_j i + r_j),$$

(3)

where r_j represents a random number while a_0 is a constant.

The results of the above prescripted surrogate test $\tilde{x}(i)$ are presented in Fig. 2b. Two signals $x(i)$ and $\tilde{x}(i)$ (Fig. 2a and b) can be easily compared through estimated statistical properties. Here we have calculated standard deviations for both time series (σ_x and $\sigma_{\tilde{x}}$) and observed that they are close to each other. This could mean that our system is influenced by a significant noisy term. Note that the surrogate test, which mixes the phases of different harmonics in random way is hardly sensitive for noisy systems. It is also possible that the examined time series differ more in higher moments. Continuing this discussion on nonlinearities in the time series, we have also plotted the return map in Fig. 3. Magnifying the scale one can see in Fig. 3b that the diagonal symmetry is barely broken. That could imply the

42

broken time reversal symmetry, which is an important effect appearing most frequently in nonlinear systems [18]. However, this effect albeit noticeable is not very clear in the present case. Thus we need another test to conclude about nonlinearity of the examined system.

On the other hand, the Fourier transform A_j (Eqs. 1-2) is presented in Fig. 4a. Note that the spectrum has a typical structure composed of a wide band and free singular frequencies related to the natural frequencies and the rotational frequency of the ripping head system (Fig. 1). Investigating further the statistical properties of the time series we have constructed its histogram which is presented in Fig. 4b. Here one can observe that the probability distribution is nonsymmetric in respect to horizontal axis. In fact, small power consumptions are more probable than higher ones. Clearly it resembles the Poisson distribution probability, which can be associated with the existence of some rare events. Naturally, the power is proportional to the torque acting on the ripping head. Thus, the increase of it can be related with the stronger resistance of the material. To explain the rock cutting process one should also take into account the nonuniform structure of rocks and cracks possibilities.
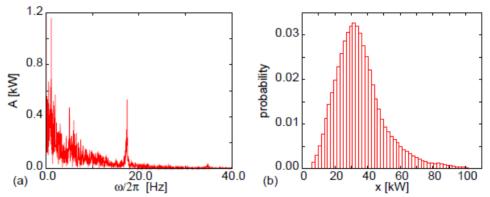

Fig. 4. Fourier transform expressed in the inverse of the sampling time unit $1/\Delta t$ ($\Delta t = 0.005s$) (a) and the related histogram of the examined time series $x(i)$ presented in Fig. 2 (b)

3. Embedding properties of the time series

We start with reconstruction of the phase space using the Takens theorem [19]. To apply this theorem we had to calculate time delay and embedding dimension. After that we will obtain a new time series which preserves topological properties of the initial one.

According to the Takens theorem [19] the nonlinear time series of single variable x_i can be represented in the reconstructed phase space as an evolution of the vector field x_i composed of the current and delayed values of the ripping head power

$$\mathbf{x}_i = \left[x_i, x_{i-\Delta i}, x_{i-2\Delta i}, ..., x_{i-(M-1)\Delta i}\right],$$

(4)

where Δi is the time delay in sampling units, M is the embedding dimension. To find Δi we use the average mutual information method (AMI) [20–22]

$$\text{AMI}(\delta i) = -\sum_{kl} p_{kl}(\delta i) \ln \frac{p_{kl}(\delta i)}{p_k p_l},$$

(5)

43

where for some partition of the ripping head power values interval $x \in [x_{min}, x_{max}]$ p_k is the probability to find a time series value in the k-th interval, and p_{kl} is the joint probability that an observation falls later into the l-th element and the observation time is given by δi. In Fig. 5a we plotted AMI versus corresponding time delay δ_i. The optimal time delay $\Delta i = \delta i$ is to be determined by AMI minimum. In our case $\Delta i = 8$ (Fig. 5a).

On the other hand, the embedding dimension can be calculated from an analysis of False Nearest Neighbors Fraction (FNNF) [22–24,8]. One has to choose the point indicated by x_i and calculate the distance to its nearest neighbor point j in the m-dimensional space; an Euclidean distance is typically used and is written as $|x_i - x_j|_m$.
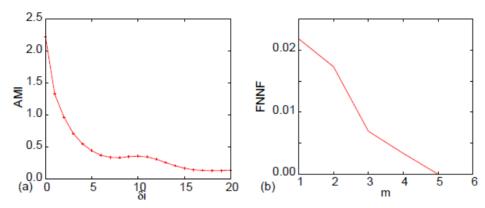

Fig. 5. The analysis of embedding: (a) Average Mutual Information – AMI versus time delay δi and (b) False Nearest Neighbour Fraction – FNNF versus embedding dimension m

Fig. 6. Function S (Eq. 8) as a function of time τ. The short straight line indicates a positive slope tendency $S \approx 0.185 \ \tau + const$ (in terms of sampling units), which indicate the positive value of the maximal Lyapunov exponent

Iterating both points along the time series we compute the control parameter $Q_{i,m}$ defined as

$$Q_{i,m} = \frac{|\mathbf{x}_i - \mathbf{x}_j|_{m+1}}{|\mathbf{x}_i - \mathbf{x}_j|_m}.$$

(6)

44

By comparing the above value to a chosen threshold Q_c, we calculate the fraction of cases for which $Q_{i,m}$ exceeds the threshold value Q_c. The FNNF can then be estimated from the following expression

$$\text{FNNF}(m) = \frac{1}{N} \sum_i \Theta(Q_{i,m} - Q_c),$$

(7)

where N is the number of vector elements in the vector time series, $\Theta(x)$ is the Heaviside step function. This so-called fraction analysis is repeated by choosing different values of the dimension m. The results of FNNF for varying m are presented in Fig. 5b. FNNF vanish for $m = 5$ and this defined the proper embedding dimension $M = 5$.

The maximal Lyapunov exponent λ_1 describes the rate of divergence of the trajectories in the phase space. The most reliable methods for estimating λ_1 for systems which can involve discontinuities (in our case generated by friction, cracks and impact phenomena) are described in [25,26,8]. Here, to calculate λ_1 we use the Kantz algorithm [25,20], which is defined in the reconstructed phase space. Following this algorithm one considers the representation of the time series data as a trajectory in the embedded space x_i, to find a close return $x_{n'}$ to a previously visited point x_n. By using the distance $x_{n'} - x_n$ as a small perturbation one checks whether the perturbation would grow exponentially in time. To estimate the growth of the perturbations, we need to compute the average for different observation points n using

$$S(\epsilon, M, \tau) = \left\langle \ln \left(\frac{1}{U_n} \sum_{\mathbf{x}_{n'} \in U_n} |\mathbf{x}_{n'+i} - \mathbf{x}_{n+i}| \right) \right\rangle_n$$

(8)

Here $U_n \sim \varepsilon^M$, being a small parameter characterizing the maximum distance around the point x_n such that $x_{n'}$ is in its vicinity ($x_{n'} \in U_n$). The slope of the linear part of S versus time τ curve yields the Lyapunov exponent.

$$\lambda_1 = \frac{\Delta S}{\Delta \tau}.$$

(9)

Using the numerical package by Hegger *et al.* [22] we have estimated S (Eq.8) as a function of time τ (in the sampling time units Δt). The results of our calculations are presented in Fig. 6. The obtained line is monotonous going up and down but for $\tau > 25$ the oscillation amplitude decreases considerably. The short straight line in Fig. 6 shows a positive slope tendency

$$S \approx 0.185\tau + \text{const},$$

(10)

which indicates the positive value of the maximal Lyapunov exponent λ_1 typical for chaotic or noisy systems.

4. Analysis of recurrence plots

Recurrence plots (RPs), which were invented by Eckmann *et al.* [27], were used later for identification of nonlinear systems with various possible behaviours [28]. Such plots are

45

constructed from a phase space vectors by spatial proximity analysis of states x_i (defined in Eq. 4). In fact using the above qualitative method for deterministic systems it is possible to classify the dynamics of an examined system by its characteristic patterns showing diagonal, vertical or horizontal structure of lines [29,30]. The same method applied to an unknown time series is capable of distinguishing chaotic and stochastic behavior. A pattern for a stochastic system is based on uniform distribution of points in the recurrence plot, while a chaotic system possesses structure of lines with finite lengths. On the other hand in a case of the intermittent motion [31], a vertical stripe structure is expected [32–35].

The recurrence plot can be defined by the following matrix form $R^{m,\varepsilon}$ with corresponding elements $R_{i,j}^{m,\varepsilon}$ [36–38]

$$R_{ij}^{m,\epsilon} = \Theta(\epsilon - |\mathbf{x_i} - \mathbf{x_j}|) \tag{11}$$

having 0 and 1 elements to be translated into the recurrence diagram as an empty place and a black dot respectively.

Using the proper embedding parameters analyzed in the previous section we have plotted the corresponding recurrence plot (in Fig. 7a) for the examined time series. Figures 7b-c show the corresponding RPs for the surrogated and autoregressive time series.

The autoregressive time series have been calculated by using the following formula

$$x_{AR}(n+1) = \sum_{i=0}^{p-1} B_i x_{AR}(n-i) + f_i, \tag{12}$$

where f_i are random numbers with Gaussian distribution of zero mean and the unit variance. In our calculations we used $p = 100$. For the best least square fit to the original time series $x(i)$ we obtained coefficients B_i, ($i = 0, ..., 99$) and presented them in Fig. 8. One can see that the first four coefficients ($|B_i| > 0.4$, $i = 0, ..., 3$) are the most important in the algorithm (Eq. 12).

For comparison we present the RP obtained for the case of random number series f_i (Fig. 7d). Note that the black points in that RP are distributed uniformly. In contrast to the uniform cover for random numbers (Fig. 7d) the other three time series Figs. 7a–c create characteristic patterns. However the original pattern for the experimental time series is partially destroyed. Especially, the vertical line structure for the surrogated data (Fig. 7b), and in the system simulated by the phenomenological auto-regression model (Eq. 12) with a random component (Fig. 7c) look differently.

Closer inspection to distinguish diagonal and horizontal lines variation may be performed by using the Recurrence Quantification Analysis (RQA). This method was invented by Webber and Zbilut [29] and later developed by Marwan [36,37].

Starting with the RQA analysis we define the recurrence rate RR:

$$RR = \frac{1}{N^2} \sum_{i,j=1}^{N} R_{ij}^{m,\epsilon}, \quad \text{for} \quad |i-j| > w \tag{13}$$

which determines the black dots fraction in the diagram. $w = 1$ denotes the Theiler window used to exclude diagonal points from the above summation (Eq. 13).

Furthermore the RQA can be used to identify vertical or diagonal lines through their maximal lengths L_{max}, V_{max} for diagonal and vertical lines respectively. In its frame, the RQA

46

enables to perform probability $p(l)$ or $p(v)$ distribution analysis of lines according to their length l or v (for diagonal and vertical lines). Practically, they are calculated

$$p(y) = \frac{P^{\epsilon}(y)}{\sum_{y=y_{min}}^{N} P^{\epsilon}(y)},$$

(14)

where $y = l$ or v depending on diagonal or vertical structures in the specific recurrence diagram. $P^{\epsilon}(y)$ denotes unnormalized probability for a given threshold value ϵ. In this way Shannon information entropies (L_{ENTR} and V_{ENTR}) can be defined for diagonal and vertical lines collections

$$L_{ENTR} = -\sum_{l=l_{min}}^{N} p(l)\ln p(l),$$

(15)

$$V_{ENTR} = -\sum_{v=v_{min}}^{N} p(v)\ln p(v).$$

(16)

Other properties as determinism DET and laminarity LAM and the trapping time TT are also basing on probabilities $P^{\epsilon}(x)$.

All the series $x(i)$, $\tilde{x}(i)$, $x_{AR}(i)$ and f_i have been renormalized by the square deviation and $RR = 0.01$ (Tab. 1).

$$DET = \frac{\sum_{l=l_{min}}^{N} l P^{\epsilon}(l)}{\sum_{i,j=1}^{N} R_{i,j}^{m,\epsilon}},$$
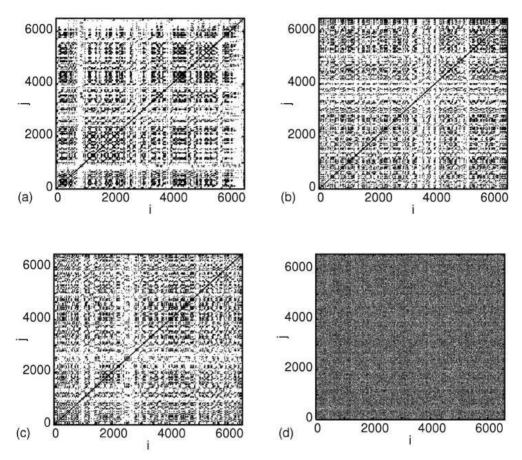
(17)

$$LAM = \frac{\sum_{v=v_{min}}^{N} v P^{\epsilon}(v)}{\sum_{v=1}^{N} v P^{\epsilon}(v)},$$

(18)

$$TT = \frac{\sum_{v=v_{min}}^{N} v P^{\epsilon}(v)}{\sum_{v=v_{min}}^{N} P^{\epsilon}(v)},$$
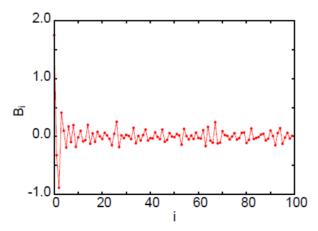
(19)

where l_{min} and v_{min} denotes minimal lengths of diagonal and vertical lines which should be chosen for a specific dynamical system.

Table 1. Summary of recurrence quantification analysis (RQA) for 'experimental', 'autoregressive' and 'surrogate' data. $w = 1$ (Theiler window) and $l_{min} = 2$, $v_{min} = 2$. Note, for all cases RR is the same.

type	RR	M	Δi	DET	LAM	L_{max}	L_{ENTR}	V_{max}	V_{ENTR}	TT
'experimental'	0.01	5	5	0.866	0.915	3611	1.799	48	1.810	3.795
'autoregressive'	0.01	5	5	0.883	0.902	684	2.121	43	1.356	1.029
'surrogate'	0.01	5	5	0.840	0.899	722	1.758	50	1.754	3.674

Fig. 7. Recurrence plots of the experimental data for the ripping head power: the experimental (a), surrogated (b) and autoregressive (c) time series and for the Gaussian noise series f_i(d)

Fig. 8. Autoregressive coefficients B_i (Eq. 12) for $p = 100$

Determinism *DET* is the measure of the predictability of the examined time series, gives the ratio of recurrent points formed in diagonals to all recurrent points. Note in a periodic system all points would be included in the lines. On the other hand laminarity *LAM* is a similar measure, which corresponds to points formed in vertical lines. This measure is telling about dynamics behind sampling points changes. For small point to point changes the consecutive points form a vertical line. Finally, trapping time *TT* refers the average length of vertical lines measuring the time scale (in terms of sampling intervals) of these small changes in the examined time history.

To express the quantitative differences between presented RPs (Fig. 7a-c) we have performed calculations of all the specified quantities (Eqs. 13,15–19) for our time series and the surrogate (Figs. 2a and b) as well as for the autoregressive simulated series and included them into Tab. 1.

Note that determinism *DET* of the 'autoregressive' time series has the largest value. It is because of a liner autoregressive model (Eq. 12) and a large number delays $p = 100$. Furthermore, *LAM* is the largest for the experimental data. This implies some vertical structure of the system dynamics. The parameters *LAM*, V_{ENTR} and *TT* (all are the largest for the original time series) are also closely related to vertical structure. Such a characteristic vertical structure appears for the intermittency phenomenon [39]. Evidently, two other examined time series ('surrogate and 'autoregressive') cannot reveal this phenomenon. Note also that the largest L_{max} = 3611 is for the experimental time series. The huge difference in L_{max} could be interpreted as the strong correlation between neighboring points. The other parameters V_{max} and L_{ENTR} reach the medium value for the original time series. Interestingly, L_{ENTR} has clearly the largest value for the autoregressive time series, informing that the noisy component f_i present in Eq. 12 can dominate here. On the other hand V_{max} is comparable to all three examined cases.

5. Summary and conclusions

We have investigated the power of a ripping head in its working conditions. Our results indicate that the system is nonlinear. This was visible in time series (Fig. 2a) analysis in terms of the return map (Fig. 3). The corresponding Fourier transform course (Fig. 4a) and the histogram graph (Fig. 4b) provided some initial insight into the noisy statistic properties of this process. Interestingly the surrogate test showed small differences in terms of square deviations. However by using some more sophisticated measures, given by recurrence plots quantification measures, we obtained obvious differences between the original and surrogated time series (see Tab.1). Finally, the examined process appeared to be completely different from the noise having some specific correlations shown also by recurrence properties (Fig. 7, Tab. 1). Using embedding methods we estimated a positive value of the maximal Lyapunov exponent demonstrating the exponential divergence typical for chaotic or stochastic systems (Fig. 6). In summary we conclude that the recurrence plots methods appeared to be a useful tool in characterizing this type of systems.

The presented methods based on the embedding theory and RQA enable to identify the complexity of the experimental signal and could be utilized in future development of the control procedure for the ripping head operation. One of advantages of the recurrence plots application is that they do not need long time series. Interestingly, this technique could be easily applied for monitoring of sudden increases of supplied power [16]. Particularly, the vertical lines parameters *LAM*, V_{ENTR} and *TT* for the original time series are the largest implying some specific behaviour of the system. This effect indicates that the dynamics of the investigated system is complex. It is also clear that apart from stochastic noise the fractal structure related to the intermittency phenomenon can be present.

References

[1] **Merchant E.M.** Mechanics of the metal cutting process, J. Appl. Phys. 11 (1945) 267–275.

[2] **Grabec I.** Chaotic dynamics of the cutting process, Int. J. Mach. Tools Manuf. 28, (1988) 19–32.

[3] **Tansel I.N., Erkal C. and Keramidas T.** The chaotic characteristics of threedimensional cutting, Int J Mach Tools Manufact 32 (1992) 811–827.

[4] **Gradisek J., Govekar E. and Grabec I.** Using coarse-grained entropy rate to detect chatter in cutting, J. Sound Vibr. 214 (1998) 941–952.

[5] **Stepan G.** Modelling nonlinear regenerative effects in metal cutting, Philos. Trans. R. Soc. Lond. A 359, (2001) 739–757.

[6] **Litak G.** Chaotic vibrations in a regenerative cutting process, Chaos, Solitons & Fractals 13 (2002) 1531–1535.

[7] **Warmi´nski J., Litak G., Cartmell M.P., Khanin R., Wiercigroch M.** Approximate analytical solutions for primary chatter in the nonlinear metal cutting model, J. Sound Vibr. 259 (2003) 917–933.

[8] **Sen A.K., Litak G., Syta A.** Cutting process dynamics by nonlinear time series and wavelet analysis, Chaos 7 (2007) 023133.

[9] **Fowell R.J.** The mechanics of rock cutting, Comprehensive Rock Engineering 4 (1993) 155–176.

[10] **Teale R.** The mechanical excavation of rock, Int. J. Rock. Mech. & Min. Science, 1 (1963) 63–64.

[11] **Eichbaum F.** Schneidend - brechende Gewinnung mit der Schneidscheibe. Experimentell und theoretische Untersuchungen. Gluckauf - Betriebsbucher, Band 22, Verlag Gluckauf GMBH Essen, 1980.

[12] **Gajewski J., Jonak J.** Utilisation of neural networks to identify the status of the cutting tool point, Tunnelling and Underground Space Technology 21 (2006) 180–184.

[13] **Jonak J., Gajewski J., Wydro T., Syta A., Nieoczym A.** The method of wear testing of tools installed on a multi-tool ripping head, Przegl¸ad Mechaniczny, 65/12S (2006), 56–58 (in Polish).

[14] **Jonak J., Gajewski J.** Identifying the cutting tool type used in excavations using neural networks, Tunnelling and Underground Space Technology 21 (2006) 185– 189.

[15] **Jonak J., Gajewski J.** Identification of ripping tool types with the use of characteristic statistical parameters of timegraphs, Tunnelling and Underground Space Technology 23 (2008) 18–24.

[16] **Litak G., Syta A., Gajewski J. and Jonak J.** Detecting and identifying nonstationary courses in the ripping head power consumption by recurrence plots, Meccanica 45 (2010) 603–608.

[17] **Schreiber T., Schmitz A.** Surrogate time series Pysica D 142 (2000) 346–382.

[18] **Sprott J.J.** Chaos and Time-Series Analysis, Oxford University Press, Oxford 2003.

[19] **Takens F.** Detecting Strange Attractors in Turbulence, Lecture Notes in Mathematics, Vol. 898 (Springer, Heidelberg 1981), pp. 366–381.

[20] **Kantz H., Schreiber T.** Non-linear Time Series Analysis, Cambridge University Press, Cambridge, 1997.

[21] **Fraser A.M. and Swinney H.L.** Independent coordinates for strange attractors from mutual information, Phys. Rev. A 33 (1986) 1134–1140.

[22] **Hegger R., Kantz H., and Schreiber T.** Practical implementation of nonlinear time series methods: The TISEAN package. CHAOS 9 (1999) 413–435.

[23] **Kennel M.B., Brown R., Abarbanel H.D.I.** Determining embedding dimension for phase-space reconstruction using a geometrical construction, Physical Review A 45 (1992) 3403–3411.

[24] **Abarbanel H.D.I.** Analysis of Observed Chaotic Data, Springer, Berlin, 1996.

[25] **Kantz H.** A robust method to estimate the maximal Lyapunov exponent of a time series, Phys. Lett. A 185 (1994) 77–87.

[26] **Rosenstein M. T., Collins J. J., De Luca C. J.** A practical method for calculating largest Lyapunov exponents from small data sets, Physica D 65 (1993) 117–134.

[27] **Eckmann J.-P., Kamphorst S.O. and Ruelle D.** Recurrence plots of dynamical systems, Europhys. Lett. 5 (1987) 973–977.

[28] **Casdagli M.C.** Recurrence plots revisited, Physica D 108 (1997) 12–44.

[29] **Webber C.L., Jr. and Zbilut J.P.** Dynamical assessment of physiological systems and states using recurrence plot strategies, J. App. Physiol. 76 (1994) 965–973.

50

[30] Marwan N., Romano M. C., Thiel M. and Kurths J. Recurrence plots for the analysis of complex systems, Physics Reports 438 (2007) 237–329.

[31] Chatterjee S., Mallik A.K. Three kinds of intermittency in a nonlinear mechanical system, Physical Review E 53 (1996) 4362–4367.

[32] Marwan N., Wessel N., Meyerfeldt U., Schirdewan A. and Kurths J. Recurrence-plot-based measures of complexity and their application to heartrate - variability data, Phys. Rev. E 66 (2002) 026702.

[33] Marwan N., Meinke A. Extended recurrence plot analysis and its application to EPR data, Int. J. Bif. and Chaos 14 (2004) 761–771.

[34] Wendeker M., Litak G., Czarnigowski J., Szabelski K. Nonperiodic oscillations of pressure in a spark ignition combustion engine, Int. J. Bif. and Chaos 14 (2004) 1801–1806.

[35] Litak G., Kami´nski T., Czarnigowski J., Zukowski D., Wendeker M. Cycle-to-cycle oscillations of heat release in a spark ignition engine, Meccanica 42 (2007) 423–433.

[36] Marwan N. Encounters with Neighbours: Current Development of Concepts Based on Recurrence Plots and their Applications, PhD Thesis, Universitat Potsdam, Potsdam 2003.

[37] Marwan N. Commandline Recurrence Plots, http://www.agnld.unipotsdam.de/~marwan/6.download/rp.php (2009-08-15).

[38] Thiel M., Romano M.C., Read P.L. and Kurths J. Estimation of dynamical invariants without embedding by recurrence plots, Chaos 14 (2004) 234–243.

[39] Litak G., Gajewski J., Syta A., Jonak J. Quantitative estimation of the tool wear effects in a ripping head by recurrence plots, Journal of Theoretical and Applied Mechanics 46 (2008) 521–530.

51